Magnetism of an adatom on bilayer graphene and its control: A first-principles perspective

Dhani Nafday and T. Saha-Dasgupta
S. N. Bose National Centre for Basic Sciences, Kolkata, India
(Received 17 September 2013; published 22 November 2013)

We present a first-principles investigation of the electronic and magnetic properties of an adatom on bilayer graphene within the framework of density functional theory. In particular, we study the influence of an applied gate voltage which modifies the electronic states of the bilayer graphene as well as shifts the adatom energy states relative to that of the graphene energy states. Our study carried out for a choice of three different adatoms, Na, Cu, and Fe, shows that the nature of adatom-graphene bonding evolves from ionic to covalent, in moving from an alkali metal, Na, to a transition metal, Cu or Fe. This leads to the formation of magnetic moments in the latter cases (Cu, Fe) and the absence of a magnetic moment in the former (Na). Application of an external electric field to bilayer graphene completely changes the scenario, switching on a magnetic moment for the Na adatom, and switching off the magnetic moments for Cu and Fe adatoms. Our results have important implications for fundamental studies of controlled adatom magnetism and spintronics applications in nanotechnology.

DOI: 10.1103/PhysRevB.88.205422 PACS number(s): 75.75.−c, 73.22.−f, 68.43.Bc, 73.20.−r

I. INTRODUCTION

It goes without saying that graphene and graphene-based structures are currently in the forefront of attention due to the wealth of properties exhibited by them, e.g., anomalous quantized Hall effect, high mobility, and carrier density controllable by external means.[1] Graphene also holds promises for spintronics.[2] As opposed to the case of diluted magnetic semiconductors,[3] where the location of impurity ions is unpredictable, adatoms can be placed on graphene in a controlled manner, using a scanning tunneling microscope.[4] The physics of an adatom on graphene has therefore been studied and explored in the context of local moment formation,[2,5] Kondo physics,[6] interaction between adatoms,[7] adatom positional ordering,[8] etc. All these studies have been carried out mostly in the context of single-layer graphene. In recent times, attention has been given to an adatom on bilayer graphene as well.[9,10] As is well known, while the single-layer graphene (SLG) is a zero-gap semiconductor with a linear Dirac-type dispersion around the Fermi energy, bilayer graphene (BLG), which is two coupled hexagonal lattices arranged according to Bernal ($\tilde{A}$-B) stacking, shows a parabolic dispersion around Fermi energy with a tiny band overlap ($\approx$0.1 meV).[11] In comparison to SLG, BLG offers an extra tuning parameter in the sense that the presence of two layers gives rise to the possibility of tuning the potential on each of the two layers of BLG individually and thereby breaking the inversion symmetry between the two layers.[12] For example, a band gap is found to open up by one-sided chemical doping of BLG,[13] or a more controlled one through an electric field applied perpendicular to a BLG sample.[14] In an adatom-BLG geometry, the application of electric field perpendicular to BLG is expected to tune the adatom energy states, in addition to the band gap opening at the Dirac point. This is due to the fact that the impurity energy level, in general, will be positioned close to the top layer of BLG on which the adatom is placed. Following this expectation, turning on and off of the local moment of an adatom on BLG by an electric field has been proposed theoretically[10] in terms of calculations within the framework of the Anderson impurity model. To the best of our knowledge, no first-principles calculation exists on the problem of an adatom on BLG in the presence of an applied electric field. A first-principles calculation which takes into account all the structural aspects, including the structural relaxation that happens due to adatom absorption, the site preference of the adatom, and the chemical aspects, correctly is expected to provide a more realistic scenario and verification of the predictions made by the model study.[10]

In this first-principles-based study, the absorption of three different metal adatoms on graphene is considered, which includes an alkali metal (Na) as well as transition metals (Cu, Fe). The magnetism of the adatom-BLG geometry, in the absence of applied electric field, is found to depend on the choice of adatom, which decides the nature of bonding between the adatom and the graphene layers. The formation of moment is found to be influenced strongly by the application of external electric field. The application of a field normal to the layers is found to turn on the magnetism in the case of Na on BLG, and turn off the magnetism for Cu as well as Fe on BLG, giving rise to the possibility of control of magnetism in adatom-BLG geometry by application of a gate voltage.

We start by giving the details of the computational technique, used in the present study in Sec. II. The result section, Sec. III, is divided into two parts. Section III A deals with the study of site preference of the adatom and the electronic structure of the adatom-BLG geometry in the absence of an applied electric field. Section III B is devoted to the main focus of the paper, the magnetism of adatom-BLG and its control by application of an external electric field. Finally, the summary and outlook are presented in Sec. IV.

II. COMPUTATIONAL DETAILS

We have carried out first-principle calculations to explore the structural, non-spin-polarized as well as spin-polarized electronic and magnetic properties of a single adatom on bilayer graphene both in the absence and in the presence of an applied electric field. Calculations have been carried out in two choices of basis sets: (a) the plane wave pseudopotential method as implemented within the Vienna *Ab initio* Package (VASP)[15] and (b) the full-potential linearized augmented plane-wave (FLAPW) method as implemented in WIEN2K.[16]

In order to model the adatom on BLG, one metal atom on a 4×4 BLG supercell was constructed with 64 carbon atoms plus one adatom in the cell, which amounts to a coverage of 1 adatom per 64 C atoms. Along the direction perpendicular to the bilayer, a 16 Å inter-bilayer distance was used in order to minimize the interactions between bilayers of neighboring supercells, due to the periodic boundary condition. To facilitate the study of the effect of the electric field, the bilayer was centered around $0.25c$, c being the length of the supercell along the z direction i.e., the direction perpendicular to the bilayer.

Structural relaxations were carried out within the density functional theory (DFT) framework as implemented in VASP. We used projected augmented wave (PAW) potentials[17] and the wave functions were expanded in the plane wave basis with a kinetic energy cutoff of 450 eV. Since the generalized gradient approximation (GGA) is known to fail for systems such as graphite or multilayer graphene, the structural relaxation was carried out within the local density approximation (LDA).[18] Within LDA, the intra-bilayer separation was found to be 3.31 Å, which is in reasonably good agreement with the experimental value of 3.33 Å for graphite, as compared to 4.21 Å obtained within GGA. The Brillouin zone (BZ) sampling was carried out with a 11×11×1 Γ-centered grid and Gaussian smearing of 0.05 eV. All the structures were optimized within the convergence criterion of 0.01 eV/Å for forces.

Ab initio DFT calculations using the all-electron method of full-potential linearized augmented plane-wave (FLAPW) as implemented in WIEN2K, were carried out on the optimized geometries obtained from plane-wave calculations for studying the electronic and magnetic properties of the adatom plus bilayer system both in the absence and in the presence of an electric field. We chose the APW + lo as the basis set. The commonly used criterion for the convergence of the basis set, relating the plane wave cutoff $K_{\max}$ and the smallest atomic sphere radius R_{MT}, $R_{MT} * K_{\max}$, was chosen to be 7.0. As in the plane-wave calculation, LDA was used for the exchange and correlation potential. To investigate the effect of an external electric field on a graphene bilayer and adatom system within the setup of three-dimensional periodic calculation, a periodic potential that is almost linear in the *relevant* region is used, as in Ref. 19. In particular, we used a periodic sawlike potential with BLG positioned in the linear region of the potential.[20] Self-consistency was carried out until the total energies were converged to within 0.001 eV. The BZ sampling is done over an 11×11×1 k mesh, as in the plane-wave calculation.

III. RESULTS

A. Site preference and electronic structure of an adatom on BLG

For a first-principles study of an adatom on graphene, it is an essential aspect to study the favorable absorption site for a given choice of adatom. In the model Hamiltonian study in Ref. 9 the adatom was assumed to be centered at C sites, while in Ref. 10 it was assumed to be positioned at the center of the hexagonal plaquette on the top layer. In reality, this should depend on the choice of adatom. We therefore start our study by calculating the site preference of the adatom.

TABLE I. The absorption energy, $E_{\rm ad}$, and the structural properties of single metal adatom adsorbed on bilayer graphene. The properties noted are adatom-carbon distance d_{ad-c} and height of adatom from the top graphene sheet $h_{\rm ad}$. $*$ implies that adatom cannot be stabilized in that specific position. For Fe and Na adatoms in bridge site, during relaxation the adatom moves to the hollow site. Similarly, Cu adatom at hollow site moves to the bridge site during relaxation.

Atom	Site	$E_{\rm ad}$ (eV)	d_{ad-c} Å	$h_{\rm ad}$
Na	H	0.668	2.560	2.117
	B*			
	T	0.542	2.391	2.339
Cu	H*			
	B	0.741	2.065	2.011
	T	0.711	1.982	2.196
Fe	H	1.763	2.055	1.439
	B*			
	T	0.760	1.843	1.626

In order to estimate the site preference of three choices of adatoms, we calculate the absorption energy, defined as[21]

$$E_{\rm ad} = E_a + E_{bg} - E_{abg},$$

where E_{abg} is the total energy of the adatom and BLG, E_a is the energy of an isolated atom, and E_{bg} is the energy of the isolated BLG, all calculated in the geometry obtained from the positions of the atoms after relaxing the adatom + BLG geometry. We consider absorption of the atom on the three sites of high symmetry, belonging to the top layer of the BLG: the hollow (H) site at the center of a hexagon, the bridge (B) site at the midpoint of a carbon-carbon bond, and the top (T) site directly above a carbon atom. Table I lists the absorption energy calculated for Na, Cu, and Fe absorbed at three different positions. The preferred site is the one which has the largest adatom absorption energy. Table I also lists the adatom vertical height ($h_{\rm ad}$) defined as the difference in z coordinate of the adatom and the average z coordinate of carbon atoms in the top layer of BLG, and the distance (d_{ad-c}) between the adatom and the nearest-neighbor C atom. We find that while Na and Fe prefer the H site, Cu prefers the B site, as shown in Fig. 1. This is similar to the findings for SLG.[21] $h_{\rm ad}$ is found to be significantly smaller for Fe compounds compared to Na, though they both prefer to sit in the H site, indicating a change in the nature of bonding between adatom and graphene, as one moves from alkali metal to transition metal.

Before we move on to the study of magnetism and the effect of external electric field on it, it is a worthwhile exercise to study the non-spin-polarized electronic structure of adatom + BLG, in order to gain knowledge about the nature of bonding between the adatom and the BLG and the perturbation caused by adatom absorption on BLG. The non-spin-polarized density of states also rationalizes the possible formation of Stoner-like instability which may drive the magnetic solution. Figure 2 shows the non-spin-polarized density of states (DOS) of the adatom on BLG, for Na, Cu, and Fe adatoms, in comparison to that of isolated BLG (shown in the topmost panel). The left panels show the DOS projected onto C atoms

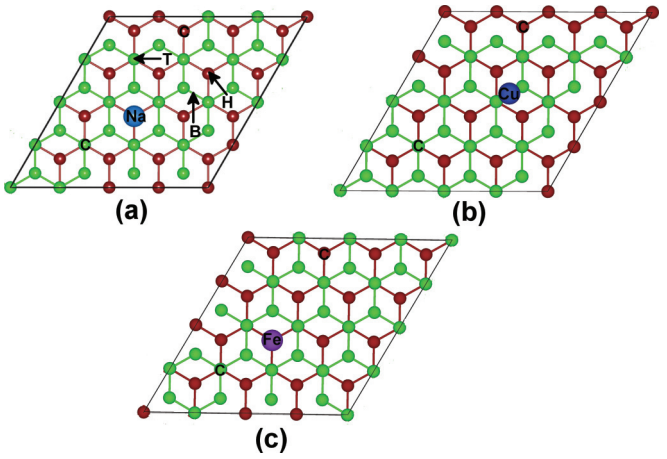

FIG. 1. (Color online) (a)–(c) The optimized geometry of adatom on BLG for (a) Na, (b) Cu, and (c) Fe. The C atoms in the top and bottom layers of BLG are colored as green/light gray and red/dark gray, respectively. The high-symmetry sites on the top layer, i.e., the H, T, and B sites, have been marked in panel (a). While Na and Fe prefer the H site, Cu sits in the B site.

in the cell and the adatom states. For Na, projection only to the Na s state is shown, while for Cu and Fe, projections to both s and d have been shown. The insets show the zoomed view of the total DOS around Fermi energy (E_F). In the right panels, projections onto C atoms belonging to the top layer and bottom layer of the BLG have been shown separately, which is expected to bring out the asymmetry between the two layers driven by the absorption of the adatom as well as the differential hybridization of the two layers to the adatom.

Focusing on the Na case first, we find that the Na s state lies above E_F, unoccupied, indicating charge transfer between the adatom and BLG. This suggests that adatom-BLG bonding is of ionic nature and close to one electron transfer from the $3s$ state of Na to graphene. This shifts E_F from the Dirac point E_D which is E_F for isolated BLG to higher energy. The addition of Na, as is clearly seen, opens up a gap (≈0.16 eV) at E_D.[22] The shape of the graphene states is found to be nearly unaltered compared to isolated BLG, indicating little or small hybridization between Na and BLG, except for the splitting between the states of the two layers due to the asymmetric charge transfer to the top and bottom layer of BLG.

For Cu, we find the Cu s state lies right at E_F while Cu d states are completely filled, positioned at an energy ≈2.5 eV below E_F. We find the projected DOS corresponding to the top layer shows significant change compared to isolated BLG with a peak right at E_F, signaling hybridization and covalent bonding with the Cu s state, while that of the bottom layer shows comparatively less influence of the adatom. The addition of Cu also opens a gap at E_D, though the size of the gap is smaller (≈0.1 eV) than that for the Na adatom, driven by increased covalency in the case of Cu, compared to Na.

Moving to the Fe adatom, we find the Fe s state to be completely empty, the charge being redistributed to Fe d–C p. The rather strong hybridization between Fe d and C p is visible, which is even stronger than that of Cu and makes the electronic structure of both top and bottom layers significantly modified, washing out the Dirac point completely. The stronger

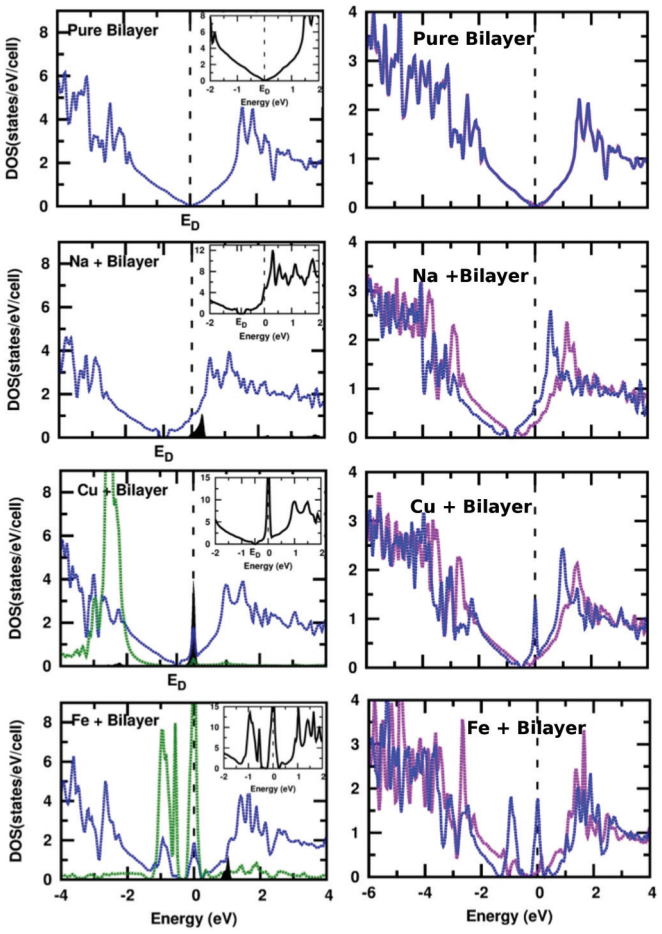

FIG. 2. (Color online) Non-spin-polarized density of states for isolated BLG, Na on BLG, Cu on BLG, and Fe on BLG (from top to bottom). The zero of the energy is set at LDA Fermi energy. The density of states presented in left panels is projected to C p states (shown as blue/dark gray solid line), adatom s state (filled area), and adatom d states (shown as green/light gray solid line). The insets show the total DOS zoomed in region close to E_F. E_D marks the Dirac point. The right panels show the individual projections to C p states belonging to top (blue/dark gray line) and bottom (magenta/light gray line) layers of the BLG.

adatom-BLG covalency for Fe compared to Cu arises due to the shorter vertical height of the adatom for Fe compared to that of Cu (cf. Table I) as well as due to different positioning of the Fe atom (H site) on BLG compared to that of Cu (B site). Fe d states are found to show a three-peaked structure. This is driven by the C_{6v} symmetry of the hollow site, which decomposes the d levels into two inequivalent two-dimensional irreducible representations E_1 (d_{yz}, d_{xz}) and E_2 ($d_{x^2-y^2}$, d_{xy}), and one one-dimensional representation A_1 ($d_{3z^2-r^2}$), with the crystal field splitting, $\epsilon_{E_2} - \epsilon_{E_1} \approx -1.0$ eV and $\epsilon_{A_1} - \epsilon_{E_1} \approx -0.7$ eV. The E_1 doublet lies at E_F, while the E_2 doublet and A_1 state are completely filled states.

The change in the nature of bonding between adatom and BLG, in moving from Na to Cu to Fe, is evident in the charge density plots, projected onto the xz plane, shown in Fig. 3. The shape of the charge density around the adatom suggests the participating orbitals in bonding for Na on BLG, Cu on BLG, and Fe on BLG to be Na s, Cu s, and Fe d, respectively.

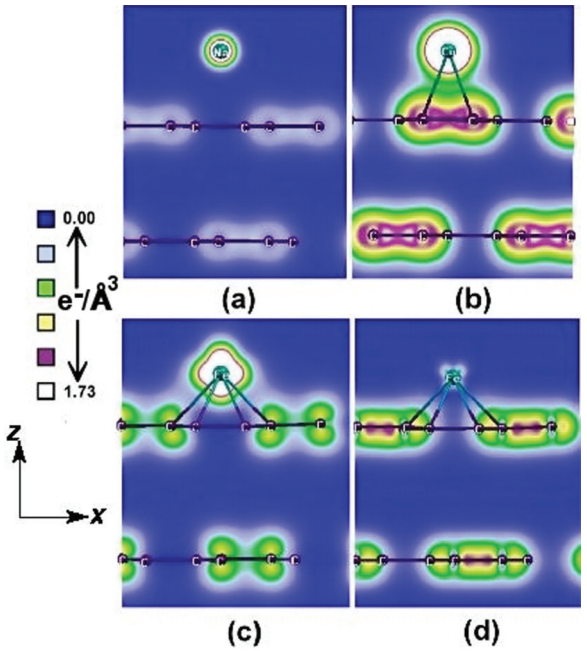

FIG. 3. (Color online) The charge density calculated for the Na on BLG, Cu on BLG, and Fe on BLG. The blue and white color represent the lowest and highest contour values [in $e^-/(\text{Å})^3$], respectively, with four intermediate contour values, as shown by the side.

For the Fe adatom, the charge density plot is shown for two chosen energy windows, one at [−0.3 eV to +0.3 eV] and another at [−0.8 eV to −1.5 eV], which has dominant Fe d_{xz}/d_{yz} and Fe $d_{x^2-y^2}/d_{xy}$ characters, respectively. The plots show the bonding with C p_z orbitals in the first case and C $sp\sigma$ orbitals in the second case. The stronger d_{xz}/d_{yz}–p_z bonding compared to that of $d_{x^2-y^2}/d_{xy}$–$sp\sigma$ is also evident.

In order to quantify the change in the nature of the bonding between the adatom and graphene layers, we computed the hybridization index as well as the charge transfer for the adatom-BLG. The hybridization index is defined as[23] $H_{\text{hyb}} = \sum_k \sum_i w^{\text{ad}}_{i,k,l} w^{C}_{i,k,p}$, where $w^{\text{ad}}_{i,k,l}$ and $w^{C}_{i,k,p}$ are the projections of the ith Kohn-Sham orbital at the kth point of the BZ onto a spherical harmonic corresponding to the lth orbital centered at the adatom and that to the p spherical harmonic centered at the nearest-neighbor C atom in the graphene layers, respectively.

Similarly, the charge transfer is defined as the charge density difference,[21]

$$\Delta\rho(\mathbf{r}) = \rho_{\text{ad-BLG}}(\mathbf{r}) - \rho_{\text{ad}}(\mathbf{r}) - \rho_{\text{BLG}}(\mathbf{r}),$$

where $\rho_{\text{ad-BLG}}(\mathbf{r})$, $\rho_{\text{ad}}(\mathbf{r})$, $\rho_{\text{BLG}}(\mathbf{r})$ are the charge densities of the adatom-BLG system, the adatom without BLG, and isolated BLG, respectively, all calculated within the same relaxed geometry as that of the adatom-BLG. In order to have a single quantitative estimate (Δq), the xy plane averaged $\Delta\bar{\rho}(z)$ was integrated from the two graphene layers to the midpoint between the averaged z coordinate of the top layer of BLG and the z coordinate of the adatom. Table II, which lists H_{hyb} as well as Δq for adatoms Na, Cu, and Fe, demonstrates the relative strengthening of the covalent character of the binding of adatom to graphene layers and the corresponding weakening of the ionic character of the same, in moving from Na to Cu to Fe. For Fe on BLG, rather strong hybridization to both top and bottom layers are observed.

TABLE II. Calculated hybridization index and the charge transfer between the adatom and the nearest-neighbor C atom belonging to graphene layers for chosen orbitals.

Adatom orbital	BLG orbital	Hybridization index	Charge transfer
Na 3s	bottom layer p	0.012	0.645
	top layer p	0.047	0.136
Cu 4s	bottom layer p	0.021	0.026
	top layer p	0.389	0.013
Fe 3d	bottom layer p	0.579	0.010
	top layer p	0.749	0.008

We note that within the periodic setup of the calculation, the adatom coverage is one adatom per 64 C atoms, and not exactly a single adatom limit, which may overemphasize the binding. However, the qualitative trend between Na, Cu, and Fe is found to be robust by comparing with the result of 3×3 supercell calculations.

B. Magnetism and effect of electric field

The non-spin-polarized DOS for both Cu on BLG and Fe on BLG show a highly peaked density of states at E_F, which according to Stoner's criteria[24] indicates instability towards magnetic solution. Following this, we carried out spin-polarized calculation for Na on BLG, Cu on BLG, and Fe on BLG. The calculated magnetic moments, as shown in Table III, show a rather small moment (≈0.2 μ_B) for Na on BLG with a tiny moment at the Na site, a moment of ≈0.95 μ_B for Cu on BLG and a rather large moment of 2 μ_B for Fe on BLG. We find that for Cu on BLG, the magnetic moment in the cell is close to 1 μ_B, the moment expected for a single unpaired electron ($S = 1/2$) in Cu 4s. For Fe on BLG, the magnetic moment of 2 μ_B is found to arise from the two unpaired electrons ($S = 1$) in the ligand field split configuration, $E_2(\uparrow\downarrow\uparrow\downarrow)\ A_1(\uparrow\downarrow)\ E_1(\uparrow\uparrow)4s^0$ with the

TABLE III. Calculated magnetic moments (in μ_B) at the adatom site, at the neighboring C atoms to the adatom, at the interstitial, and the total magnetic moment within the cell, calculated without application of electric field. Interstitial refers to the region in between atom-centered muffin-tin spheres, used in the LAPW calculation.

Site	Magnetic Moment		
	Na + bilayer	Cu + bilayer	Fe + bilayer
Carbon	0.0002	0.0079	0.0135
	0.0002	0.0080	0.0135
	0.0002	0.0050	0.0135
	0.0002	0.0049	0.0135
	0.0002	0.0083	0.0135
	0.0002	0.0084	0.0135
	0.0001	0.0002	0.0004
Adatom	0.0230	0.6951	1.8403
Interstitial	0.1650	0.1980	0.1745
Total	0.1870	0.9492	2.0000

magnetism arising due to spin residing in E_1 orbital. We note that the $E_1(\uparrow\uparrow)$ configuration leads to an orbitally quenched situation with the effect of spin-orbit coupling (SOC) being minimal. The comparatively large moments at neighboring C atoms are observed for Fe on BLG, compared to Cu on BLG or Na on BLG, indicating again large hybridization between Fe adatom and neighboring C atoms. For Na on BLG, on the other hand, we find that the net moment in the cell is much smaller than the expected moment of 1 μ_B from a single unpaired electron in the Na 3s shell. This happens due to the fact that the transferred electron from the Na 3s shell gets distributed among the C atoms in the graphene layers which provide an sp-bonded wide bandwidth that is unable to a support local moment. On the other hand, the positioning of Cu s or Fe d levels with respect to C sp levels is such that a covalent bond is formed between the adatom and the neighboring C atoms in the graphene layer with small or practically no transfer of electron from the adatom. The computed electronic structure in such cases is close to the scenario of the Anderson impurity model. The unpaired electron/electrons from the adatom are contained mostly in the sharply peaked DOS at E_F with a small bandwidth of 0.5 eV or less, supporting the formation of a local moment. The $S = 1$ state in the d^8 configuration, as found for Fe on BLG, has been discussed in the context of Co on SLG.[25] For such a scenario, a rather high Kondo temperature has been predicted, which may be applicable for Fe on BLG.

The formation of the moment, which is dependent on the relative positioning of the adatom energy levels with respect to that of C energy levels, may be tuned through an external electric field, applied perpendicular to the BLG layers. In the next step, we therefore carried out calculation in the presence of finite electric field. To validate the reliability of our calculation, we first calculated the electronic structure of isolated BLG in the absence and in the presence of finite electric field. The calculated DOS and band structures are shown in Fig. 4, for $U_{\rm ext} = 0$ eV and 1 eV, where $U_{\rm ext}$ is defined as $e \times E^z_{ex} \times d$, E^z_{ex} being the external electric field along the z direction and d being the intralayer separation of BLG (set at 3.31 Å). Our results reproduce the previously found theoretical[20] and experimental[13] results that application of finite electric field opens up a gap at the Dirac point. For $U_{ex} = 1$ eV, the low-energy spectrum is found to develop a Mexican hat structure with a gap value of ≈0.25 eV, in good agreement with previous first-principles reports.[20] The application of the electric field makes the top and bottom layers asymmetric, as found from the projected DOS.

The results of application of the external electric field on the adatom on BLG is presented in Fig. 5, which shows the non-spin-polarized density of states projected onto adatom states and C atoms of BLG, for various different values of the external electric field. The left panels are for Na on BLG while the right panels are for Cu on BLG. Focusing on the Na case first, we find that application of the electric field moves the position of the Na s level to lower energy, and for the choice of $U_{\rm ext} = 3$ eV, the half-filled Na s level lies right at E_F, making the situation comparable to Cu on BLG, in the absence of an electric field. The presence of a finite electric field, though, makes the asymmetry between the top and bottom layer of BLG states (not shown in the figure) to

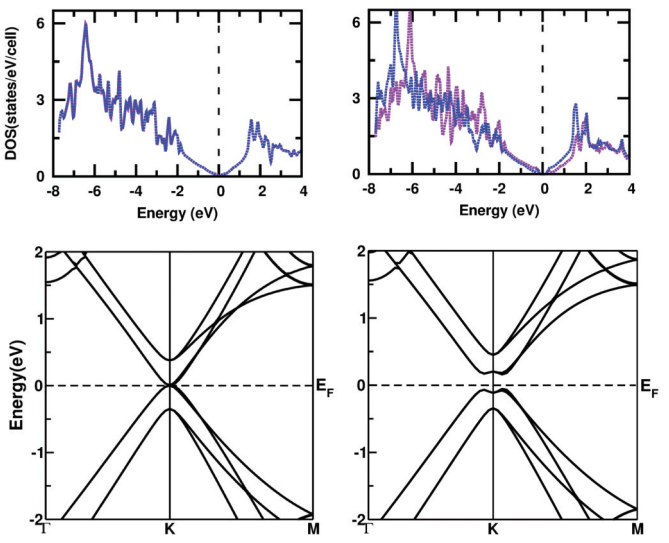

FIG. 4. (Color online) The density of states (top panels) and the band structure (bottom panels) of isolated BLG in absence (left panels) and in presence of an external electric field of strength $U_{\rm ext} = 1$ eV (right panels). Density of states has been projected onto the top and bottom layers (shown as blue/dark gray and magenta/light gray colored lines, which fall on top of each other for the BLG in absence of electric field.

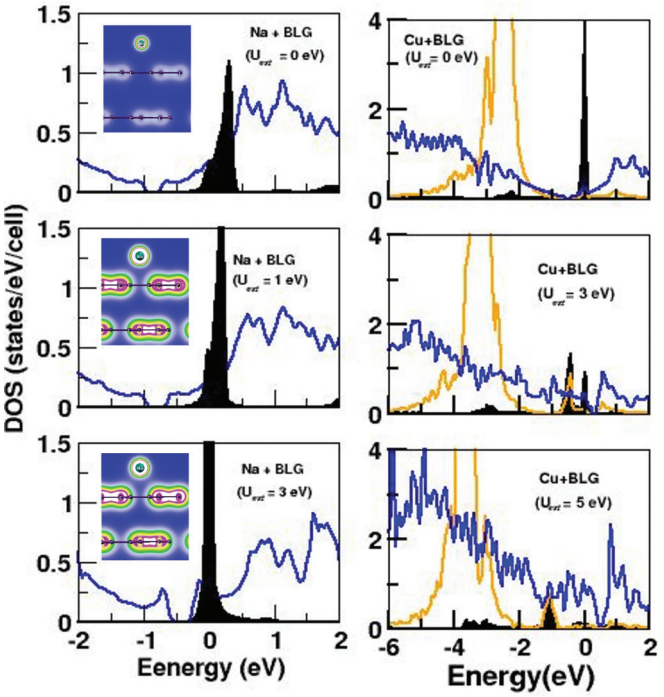

FIG. 5. (Color online) Non-spin-polarized density of states for Na on BLG (left panels) and Cu on BLG (right panels) for increasing values of external electric field. The density of states is projected to C states (shown as blue/dark gray, solid lines), adatom s state (filled area), and adatom d states (shown as orange/thin light gray, solid line). For better visibility of adatom s states, the C states have been scaled down by a factor of 4. The insets in left panels show the charge density plots for Na on BLG for corresponding values of applied electric field. The contour values are as in Fig. 3.

TABLE IV. Calculated magnetic moments (in μ_B) at the adatom site, at the neighboring C atoms to the adatom, at the interstitial, and the total magnetic moment within the cell, calculated for various different values of external electric field. Interstitial refers to the region in between atom-centered muffin-tin spheres, used in the LAPW calculation.

	Na + bilayer			Cu + bilayer			Fe + bilayer		
	Magnetic moment			Magnetic moment			Magnetic moment		
U_{ext}	0 eV	1 eV	3 eV	0 eV	3 eV	5 eV	0 eV	3 eV	5 eV
C (nn)	0.0001	0.0006	0.0020	0.0079	0.0013	0.0001	0.0135	0.0086	0.0009
	0.0002	0.0005	0.0020	0.0080	0.0010	0.0000	0.0135	0.0086	0.0009
	0.0002	0.0004	0.0020	0.0050	0.0180	0.0001	0.0135	0.0086	0.0009
	0.0004	0.0005	0.0036	0.0049	0.0137	0.0001	0.0135	0.0085	0.0009
	0.0003	0.0006	0.0037	0.0083	0.0011	0.0025	0.0135	0.0085	0.0009
	0.0003	0.0007	0.0037	0.0084	0.0009	0.0001	0.0135	0.0085	0.0009
	0.0001	0.0001	0.0005	0.0002	0.0017	0.0001	0.0004	0.0008	0.0001
Adatom	0.023	0.043	0.325	0.695	0.453	0.0017	1.840	1.017	0.113
Interstitial	0.165	0.204	0.605	0.198	0.164	0.0252	0.174	0.087	0.032
Total	0.187	0.251	0.951	0.949	0.685	0.032	2.000	0.807	0.129

be more pronounced compared to Cu on BLG in the absence of electric field. The plot of the charge density, shown as insets, demonstrates further the change in the nature of the bonding of the Na adatom to BLG from ionic to covalent like upon application of electric field. This results in electric field assisted turning on of the magnetic moment considering the spin-polarized calculation, as found from the moments listed in Table IV. For $U_{ext} = 3$ eV, the calculated moment is found to be as large as 0.95 μ_B, very close to fully polarized moment of 1 μ_B, arising out of one unpaired electron. For Cu on BLG, on the other hand, the application of electric field moves the peak corresponding to Cu 4*s* away from E_F, making it more occupied with charge transfer from graphene layer to Cu *s*. This is reflected in the computed magnetic moment which drops from a value of 0.95 μ_B for $U_{eff} = 0$ eV to 0.68 μ_B for $U_{eff} = 3$ eV to a tiny value of 0.03 μ_B for $U_{eff} = 5$ eV. The Cu *d* states also show a downward shift upon application of electric field, remaining always fully occupied.

The movement of Na *s* and Cu *s* upon increasing value of the external electric field is therefore complementary. While for Na on BLG, the increasing electric field shifts the Na *s* level closer to E_F, making it from empty to a half-filled state, for Cu on BLG the electric field shifts the Cu *s* level away from E_F, making it from half-filled to filled state, as is schematically shown in Fig. 6.

Figure 7 shows the effect of application of external electric field for Fe on BLG. As we find from Fig. 7, application of the external electric field almost rigidly shifts the position of Fe *d* states, maintaining the three-peaked structure with peak widths and the crystal field splitting nearly the same. This causes the value of the total density of states at E_F, $N(E_F)$, to drop from a value of ≈35 states/eV/cell, for $U_{ext} = 0$ eV, to ≈15 states/eV/cell for $U_{ext} = 3$ eV, to ≈4 states/eV/cell for $U_{ext} = 5$ eV, making magnetism less and less favorable. This is shown in the last columns of Table IV, which shows a fall of magnetic moment from a value of 2 μ_B for $U_{ext} = 0$ eV, to ≈0.8 μ_B for $U_{ext} = 3$ eV, to a value of ≈0.13 μ_B for $U_{ext} = 5$ eV. The nominal valence configuration of Fe, as gathered from Fig. 7, evolves from $S = 1$ d^8 to $S = 1/2$ d^9 to $S = 0$ d^{10} configuration, upon increasing the electric field value from $U_{ext} = 0$ eV to 3 eV to 5 eV. This is driven by the charge transfer from BLG to Fe, triggered by the relative movement of Fe *d* energy level positions with respect to C states. The d^9 like configuration of Fe for $U_{ext} = 3$ eV, with an unpaired electron in the doubly degenerate E_1 state, is expected to be orbitally active. Following this, one would expect the role of SOC to be important. In order to check this, we repeated the calculation in the presence of SOC. The calculated spin and orbital moment at the Fe site turned out to be 0.98 μ_B and 0.22 μ_B, respectively, with the spin and orbital moments aligned in the same direction, in accordance with the more than half-filled nature of Fe *d* states. This would lift the fourfold degeneracy of E_1 states into a twofold-degenerate ground state, separated from a twofold-degenerate excited state, with important implication for Kondo physics.[25]

Finally, a strong correlation effect becomes important in describing phenomena such as the multichannel Kondo effect and the associated non-Fermi-liquid behavior, observed for magnetic adatoms on graphene. However, the present computational framework is not a suitable framework in which

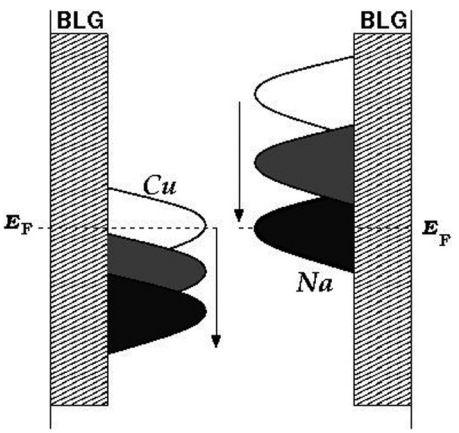

FIG. 6. Schematic diagram showing the movement of Cu *s* state and Na *s* state on BLG, upon application of increasing electric field. The direction of increase of electric field in two cases is shown with arrows.

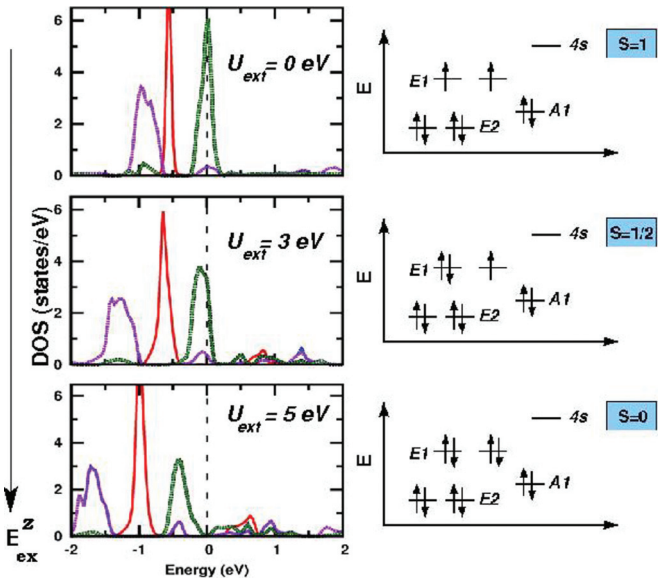

FIG. 7. (Color online) Non-spin-polarized density of states for Fe on BLG for external electric field of increasing strength ($U_{\text{ext}} = 0$ eV, 3 eV, and 5 eV, from top to bottom). The left panels show the density of states projected to Fe E_2 (magenta/dark, gray line), A_1 (red/light gray line), and E_1 (green/thick, gray line) states. The right panels show the corresponding energy level diagrams at Fe site and their occupancies.

to address that. For that one needs to include dynamical treatment of the strongly interacting $3d$ electrons, as carried out in Ref. 6, or the renormalization group treatment as carried out in Ref. 25. We have also carried out LDA + U calculations, with a choice of $U = 4$ eV and $J_H = 0.9$ eV, applied at the Fe site. The LDA and LDA + U results are found to be very similar with respect to magnetic moments and occupations of the Fe d levels. Compared to the LDA results, LDA + U results tend to show a slightly higher moment at the Fe site (e.g., 1.91 μ_B at the Fe site in LDA + U compared to 1.84 μ_B in the LDA calculation, for $U_{\text{ext}} = 0$ eV; 1.12 μ_B at the Fe site in LDA + U compared to 1.017 μ_B in the LDA calculation, for electric field $U_{\text{ext}} = 3$ eV), without changing the basic conclusion. This trend is expected and in good agreement with findings in Ref. 6, where GGA and the B3LYP hybrid functional (combination of GGA and Hartee-Fock exchange-correlation functional)[26] results were found to be remarkably similar, confirming that the static, mean-field way of handling correlation has little effect, and the basic electronic structure is described well by the band structure method, as far as the magnetic moments and d occupancies are considered.

IV. SUMMARY AND OUTLOOK

Employing density functional theory, we study the absorption of an alkali-metal adatom such as Na and transition-metal adatoms such as Cu and Fe on bilayer graphene, with the aim of studying the formation of the local moment. This encompasses single-orbital cases such as Na, Cu, for which it is the s orbital of the adatom that plays the key role in magnetism, as well as multiorbital situations such as Fe, for which it is the d-orbital manifold of the adatom that plays the key role. We study the absorption geometry, the basic electronic structure, and the bonding properties of adatom-BLG. Our study reveals that ionic bonding between Na and BLG disfavors formation of a local moment, while the covalent nature of bonding with minimal charge transfer between adatom and BLG, as in the case of Cu and Fe, promotes formation of a local moment. This scenario is affected strongly by switching on an external electric field, applied perpendicular to layers. The external electric field, in addition to affecting the electronic structure of BLG, moves the adatom energy positions with respect to graphene energy states, thereby changing the character of adatom-BLG bonding from ionic to more covalent-like, and vice versa. This switches on and off the adatom magnetism. Note that the strength of the electric field, for switching on and off the magnetism, predicted by DFT is found to be rather large, which presumably originates partly due to stronger screening in DFT.[20] Considering the state-of-the-art experimental condition, the effect reported in our study should be observable in the laboratory.

In the next stage, we wish to carry forward this study for the case of a pair of adatoms and the interaction between them. As predicted by the model calculation,[10] with the help of an electric field, it might be possible to tune the strength as well as the sign of the RKKY interaction that may be effective between two adatoms. It will be a worthwhile exercise to study this taking into account the realistic effects of chemistry and structure.

ACKNOWLEDGMENTS

The authors thank the Ministry of Earth Science and Department of Science and Technology, India, for financial support. The authors acknowledge useful discussion with A. Paramekanti.

[1] K. S. Novoselov, A. K. Geim, S. V. Morozov, D. Jiang, Y. Zhang, S. V. Dubonos, I. V. Gregorieva, and A. A. Firsov, Science **306**, 666 (2004); Y. Zhang, Y. W. Tan, H. L. Stormer, and P. Kim, Nature (London) **438**, 201 (2005); A. K. Geim and S. K. Novoselov, Nat. Mater. **6**, 183 (2007).

[2] B. Uchoa, V. N. Kotov, N. M. R. Peres, and A. H. Castro Neto, Phys. Rev. Lett. **101**, 026805 (2008).

[3] A. H. MacDonald, P. Schiffer, and N. Samarth, Nat. Mater. **4**, 195 (2005).

[4] D. M. Eigler and E. K. Schweizer, Nature (London) **344**, 524 (1990).

[5] P. Venezuela, R. B. Muniz, A. T. Costa, D. M. Edwards, S. R. Power, and M. S. Ferreira, Phys. Rev. B **80**, 241413 (2009).

[6] D. Jacob and G. Kotliar, Phys. Rev. B **82**, 085423 (2010).

[7] S. Saremi, Phys. Rev. B **76**, 184430 (2007); V. K. Dugaev, V. I. Litvinov, and J. Barnas, *ibid.* **74**, 224438 (2006).

[8] J. Berashevich and T. Chakraborty, Phys. Rev. B **80**, 033404 (2009).

[9] K.-H. Ding, Z.-G. Zhu, and J. Berakdar, J. Phys.: Condens. Matter **21**, 182002 (2009).

[10] M. Killi, D. Heidarian, and A. Paramekanti, New J. Phys. **13**, 053043 (2011).

[11]B. Partoens and F. M. Peeters, Phys. Rev. B **74**, 075404 (2006).
[12]J. Zheng, Y. Wang, L. Wang, R. Quhe, Z. Ni, W.-N. Mei, Z. Gao, D. Yu, J. Shi, and J. Lu, Sci. Rep. **3**, 2081 (2013); R. Quhe, J. Ma, Z. Zeng, K. Tang, J. Zheng, Y. Wang, Z. Ni, L. Wang, Z. Gao, J. Shi, and J. Lu, *ibid.* **3**, 1794 (2013).
[13]T. Ohta, A. Bostwick, T. Seyller, K. Horn, and E. Rotenberg, Science **313**, 951 (2006); S. Y. Zhou, G. H. Gweon, A. V. Fedorov, P. N. First, W. A. de Heer, D. H. Lee, F. Guinea, A. H. Castro Neto, and A. Lanzara, Nat. Mater. **6**, 770 (2007).
[14]Y. B. Zhang, T. T. Tang, C. Girit, Z. Hao, M. C. Martin, A. Zettl, M. F. Crommie, Y. R. Shen, and F. Wang, Nature (London) **459**, 820 (2009).
[15]G. Kresse and J. Hafner, Phys. Rev. B **47**, 558 (1993); G. Kresse and J. Furthmüller, *ibid.* **54**, 11169 (1996).
[16]P. Blaha, K. Schwarz, G. K. H. Masden, D. Kvasnicka, and J. Luitz, *Wien2k, An Augumented Plane Wave + Local Orbitals Program for Calculating Crystal Properties*, edited by K. Schwarz (Technische Universitiät Wien, Vienna, 2001).
[17]P. E. Blöchl, Phys. Rev. B **50**, 17953 (1994); G. Kresse and D. Joubert, *ibid.* **59**, 1758 (1999).
[18]N. Ooi, A. Raikar, and J. B. Adams, Carbon **44**, 231 (2006).
[19]J. Stahn, U. Pietsch, P. Blaha, and K. Schwarz, Phys. Rev. B **63**, 165205 (2001).
[20]H. Min, B. Sahu, S. K. Banerjee, and A. H. MacDonald, Phys. Rev. B **75**, 155115 (2007).
[21]K. T. Chan, J. B. Neaton, and M. L. Cohen, Phys. Rev. B **77**, 235430 (2008).
[22]This gap may be viewed as a local gap or gap opened by a periodic placing of adatoms on BLG.
[23]H. Häkkinen, M. Moseler, and U. Landman, Phys. Rev. Lett. **89**, 033401 (2002); H. Häkkinen, B. Yoon, U. Landman, X. Li, H.-J. Zhai, and L.-S. Wang, J. Phys. Chem. A, **107**, 6168 (2003).
[24]E. C. Stoner, Proc. R. Soc. London, Ser. A **165**, 372 (1938).
[25]T. O. Wehling, A. V. Balatsky, M. I. Katsnelson, A. I. Lichtenstein, and A. Rosch, Phys. Rev. B **81**, 115427 (2010).
[26]A. D. Becke, J. Chem. Phys. **98**, 5648 (1993).